

Casimir forces in the time domain: TheoryAlejandro W. Rodriguez,¹ Alexander P. McCauley,¹ John D. Joannopoulos,¹ and Steven G. Johnson²¹*Department of Physics, Massachusetts Institute of Technology, Cambridge, Massachusetts 02139, USA*²*Department of Mathematics, Massachusetts Institute of Technology, Cambridge, Massachusetts 02139, USA*

(Received 1 April 2009; published 27 July 2009)

We present a method to compute Casimir forces in arbitrary geometries and for arbitrary materials based on the finite-difference time-domain (FDTD) scheme. The method involves the time evolution of electric and magnetic fields in response to a set of current sources, in a modified medium with frequency-independent conductivity. The advantage of this approach is that it allows one to exploit existing FDTD software, without modification, to compute Casimir forces. In this paper, we focus on the derivation, implementation choices, and essential properties of the time-domain algorithm, both considered analytically and illustrated in the simplest parallel-plate geometry.

DOI: [10.1103/PhysRevA.80.012115](https://doi.org/10.1103/PhysRevA.80.012115)

PACS number(s): 12.20.-m, 02.70.-c, 42.50.Ct, 42.50.Lc

I. INTRODUCTION

In recent years, Casimir forces arising from quantum vacuum fluctuations of the electromagnetic field [1–3] have become the focus of intense theoretical and experimental effort [4–21]. This effect has been verified via many experiments [22–25], most commonly in simple, one-dimensional geometries involving parallel plates or approximations thereof, with some exceptions [26]. A particular topic of interest is the geometry and material dependence of the force, a subject that has only recently begun to be addressed in experiments [26] and by promising new theoretical methods [27–38]. For example, recent works have shown that it is possible to find unusual effects arising from many-body interactions or from systems exhibiting strongly coupled material and geometric dispersion [39–43]. These numerical studies have been mainly focused in two-dimensional [13,44–46] or simple three-dimensional constant-cross-section geometries [33,40,47] for which numerical calculations are tractable.

In this paper, we present a simple and general method to compute Casimir forces in arbitrary geometries and for arbitrary materials that is based on a finite-difference time-domain (FDTD) scheme in which Maxwell's equations are evolved in time [48]. A time-domain approach offers a number of advantages over previous methods. First, and foremost, it enables researchers to exploit powerful free and commercial FDTD software with no modification. The generality of many available FDTD solvers provides yet another means to explore the material and geometry dependence of the force, including calculations involving anisotropic dielectrics [49] and/or three-dimensional problems. Second, this formulation also offers a fundamentally different viewpoint on Casimir phenomena, and thus new opportunities for the theoretical and numerical understanding of the force in complex geometries.

Our time-domain method is based on a standard formulation in which the Casimir force is expressed as a contour integral of the frequency-domain stress tensor [2]. Like most other methods for Casimir calculations, the stress-tensor method typically involves evaluation at imaginary frequencies, which we show to be unsuitable for FDTD. We over-

come this difficulty by exploiting a recently developed exact equivalence between the system for which we wish to compute the Casimir force and a transformed problem in which all material properties are modified to include dissipation [50]. To illustrate this approach, we consider a simple choice of contour, corresponding to a conductive medium that leads to a simple and efficient time-domain implementation. Finally, using a free, widely available FDTD code [51], we compute the force between two vacuum-separated perfectly metallic plates, a geometry that is amenable to analytical calculations and which we use to analyze various important features of our method. An illustration of the power and flexibility of this method will be provided in a planned subsequent article [52], in which we will demonstrate computations of the force in a number of nontrivial (dispersive, three-dimensional) geometries as well as further refinements to the method.

II. METHOD

In what follows, we derive a numerical method to compute the Casimir force on a body using the FDTD method. The basic steps involved in computing the force are:

(i) Map the problem exactly onto a new problem with dissipation given by a frequency-independent conductivity σ .

(ii) Measure the electric \mathbf{E} and magnetic \mathbf{H} fields in response to current pulses placed separately at each point along a surface enclosing the body of interest.

(iii) Integrate these fields in space over the enclosing surface and then integrate this result, multiplied by a known function $g(-t)$, over time t , via Eq. (29).

The result of this process is the exact Casimir force (in the limit of sufficient computational resolution), expressed via Eq. (29) and requiring only the time-evolution of Eqs. (15) and (16).

In this section, we describe the mathematical development of our time-domain computational method, starting from a standard formulation in which the Casimir force is expressed as a contour integral of the frequency-domain stress tensor. We consider the frequency domain for derivation purposes only since the final technique outlined above resides entirely in the time domain. In this framework, computing the Ca-

simir force involves the repeated evaluation of the photon Green's function G_{ij} over a surface S surrounding the object of interest. Our goal is then to compute G_{ij} via the FDTD method. The straightforward way to achieve this involves computing the Fourier transform of the electric field in response to a short pulse. However, in most methods a crucial step for evaluating the resulting frequency integral is the passage to imaginary frequencies, corresponding to imaginary time. We show that, in the FDTD, this gives rise to exponentially growing solutions and is therefore unsuitable. Instead, we describe an alternative formulation of the problem that exploits a recently proposed equivalence in which contour deformations in the complex frequency-domain $\omega(\xi)$ correspond to introducing an effective dispersive, dissipative medium at a real "frequency" ξ . From this perspective, it becomes simple to modify the FDTD Maxwell's equations for the purpose of obtaining well-behaved stress-tensor frequency integrands. We illustrate our approach by considering a contour corresponding to a medium with frequency-independent conductivity σ . This contour has the advantage of being easily implemented in the FDTD, and in fact is already incorporated in most FDTD solvers. Finally, we show that it is possible to abandon the frequency domain entirely in favor of evaluating the force integral directly in the time domain, which offers several conceptual and numerical advantages.

A. Stress-tensor formulation

The Casimir force on a body can be expressed [2] as an integral over any closed surface S (enclosing the body) of the mean electromagnetic stress tensor $\langle T_{ij}(\mathbf{r}, \omega) \rangle$. Here \mathbf{r} denotes spatial position and ω frequency. In particular, the force in the i th direction is given by

$$F_i = \int_0^\infty d\omega \oint_S \sum_j \langle T_{ij}(\mathbf{r}, \omega) \rangle dS_j, \quad (1)$$

The stress tensor is expressed in terms of correlation functions of the field operators $\langle E_i(\mathbf{r}, \omega) E_j(\mathbf{r}', \omega) \rangle$ and $\langle H_i(\mathbf{r}, \omega) H_j(\mathbf{r}', \omega) \rangle$,

$$\begin{aligned} \langle T_{ij}(\mathbf{r}, \omega) \rangle = & \mu(\mathbf{r}, \omega) \left[\langle H_i(\mathbf{r}) H_j(\mathbf{r}) \rangle_\omega - \frac{1}{2} \delta_{ij} \sum_k \langle H_k(\mathbf{r}) H_k(\mathbf{r}) \rangle_\omega \right] \\ & + \varepsilon(\mathbf{r}, \omega) \left[\langle E_i(\mathbf{r}) E_j(\mathbf{r}) \rangle_\omega \right. \\ & \left. - \frac{1}{2} \delta_{ij} \sum_k \langle E_k(\mathbf{r}) E_k(\mathbf{r}) \rangle_\omega \right], \quad (2) \end{aligned}$$

where both the electric and magnetic-field correlation functions can be written as derivatives of a vector potential operator $\mathbf{A}^E(\mathbf{r}, \omega)$,

$$E_i(\mathbf{r}, \omega) = -i\omega A_i^E(\mathbf{r}, \omega), \quad (3)$$

$$\mu H_i(\mathbf{r}, \omega) = (\nabla \times)_{ij} A_j^E(\mathbf{r}, \omega). \quad (4)$$

We explicitly place a superscript on the vector potential in order to refer to our choice of gauge [Eqs. (3) and (4)], in

which \mathbf{E} is obtained as a time derivative of \mathbf{A} . The fluctuation-dissipation theorem relates the correlation function of \mathbf{A}^E to the photon Green's function $G_{ij}^E(\omega; \mathbf{r}, \mathbf{r}')$,

$$\langle A_i^E(\mathbf{r}, \omega) A_j^E(\mathbf{r}', \omega) \rangle = -\frac{\hbar}{\pi} \text{Im} G_{ij}^E(\omega; \mathbf{r}, \mathbf{r}'), \quad (5)$$

where G_{ij}^E is the vector potential A_i^E in response to an electric-dipole current \mathbf{J} along the $\hat{\mathbf{e}}_j$ direction,

$$\left[\nabla \times \frac{1}{\mu(\mathbf{r}, \omega)} \nabla \times - \omega^2 \varepsilon(\mathbf{r}, \omega) \right] \mathbf{G}_j^E(\omega; \mathbf{r}, \mathbf{r}') = \delta(\mathbf{r} - \mathbf{r}') \hat{\mathbf{e}}_j, \quad (6)$$

Given G_{ij}^E , one can use Eqs. (3) and (4) in conjunction with Eq. (5) to express the field correlation functions at points \mathbf{r} and \mathbf{r}' in terms of the photon Green's function,

$$\langle E_i(\mathbf{r}, \omega) E_j(\mathbf{r}', \omega) \rangle = \frac{\hbar}{\pi} \omega^2 \text{Im} G_{ij}^E(\omega; \mathbf{r}, \mathbf{r}'), \quad (7)$$

$$\langle H_i(\mathbf{r}, \omega) H_j(\mathbf{r}', \omega) \rangle = -\frac{\hbar}{\pi} (\nabla \times)_{il} (\nabla \times)_{jm} \text{Im} G_{lm}^E(\mathbf{r}, \mathbf{r}', \omega), \quad (8)$$

In order to find the force via Eq. (1), we must first compute $G_{ij}^E(\mathbf{r}, \mathbf{r}' = \mathbf{r}, \omega)$ at every \mathbf{r} on the surface of integration S , and for every ω [2]. Equation (6) can be solved numerically in a number of ways, such as by a finite-difference discretization [30]: this involves discretizing space and solving the resulting matrix eigenvalue equation using standard numerical linear algebra techniques [53,54]. We note that finite spatial discretization automatically regularizes the singularity in G_{ij}^E at $\mathbf{r} = \mathbf{r}'$, making G_{ij}^E finite everywhere [30].

B. Complex frequency domain

The present form of Eq. (6) is of limited computational utility because it gives rise to an oscillatory integrand with non-negligible contributions at all frequencies, making numerical integration difficult [30]. However, the integral over ω can be re-expressed as the imaginary part of a contour integral of an analytic function by commuting the ω integration with the Im operator in Eqs. (7) and (8). Physical causality implies that there can be no poles in the integrand in the upper complex plane. The integral, considered as a complex contour integral, is then invariant if the contour of integration is deformed above the real-frequency axis and into the first quadrant of the complex-frequency plane, via some mapping $\omega \rightarrow \omega(\xi)$. This allows us to add a positive imaginary component to the frequency, which causes the force integrand to decay rapidly with increasing ξ [50]. In particular, upon deformation, Eq. (6) is mapped to

$$\left[\nabla \times \frac{1}{\mu(\mathbf{r}, \omega)} \nabla \times - \omega^2(\xi) \varepsilon(\mathbf{r}, \omega) \right] \mathbf{G}_j^E(\xi; \mathbf{r}, \mathbf{r}') = \delta(\mathbf{r} - \mathbf{r}') \hat{\mathbf{e}}_j, \quad (9)$$

and Eqs. (7) and (8) are mapped to

$$\langle E_i(\mathbf{r}, \omega) E_j(\mathbf{r}', \omega) \rangle = \frac{\hbar}{\pi} \omega^2 G_{ij}^E(\omega; \mathbf{r}, \mathbf{r}'), \quad (10)$$

$$\langle H_i(\mathbf{r}, \omega) H_j(\mathbf{r}', \omega) \rangle = -\frac{\hbar}{\pi} (\nabla \times)_{ii} (\nabla' \times)_{jm} G_{lm}^E(\mathbf{r}, \mathbf{r}', \omega), \quad (11)$$

Equation (1) becomes

$$F_i = \text{Im} \int_0^\infty d\xi \frac{d\omega}{d\xi} \oint_{\text{surface}} \sum_j \langle T_{ij}(\mathbf{r}, \omega) \rangle dS_j, \quad (12)$$

[Note that a finite spatial grid (as used in the present approach) requires no further regularization of the integrand, and the finite value of all quantities means there is no difficulty in commuting the Im operator with the integration.]

We can choose from a general class of contours, provided that they satisfy $\omega(0)=0$ and remain above the real ξ axis. The standard contour $\omega(\xi)=i\xi$ is a Wick rotation, which is known to yield a force integrand that is smooth and exponentially decaying in ξ [2]. In general, the most suitable contour will depend on the numerical method being employed. A Wick rotation guarantees a strictly positive-definite and real-symmetric Green's function, making Eq. (6) solvable by the most efficient numerical techniques (e.g., the conjugate-gradient method) [54]. One can also solve Eq. (6) for arbitrary $\omega(\xi)$ [50], but this will generally involve the use of direct solvers or more complicated iterative techniques [53]. However, the class of contours amenable to an efficient time-domain solution is more restricted. For instance, a Wick rotation turns out to be unstable in the time domain because it implies the presence of gain [50].

C. Time-domain approach

It is possible to solve Eq. (6) in the time domain by evolving Maxwell's equations in response to a delta-function current impulse $\mathbf{J}(\mathbf{r}, t) = \delta(\mathbf{r} - \mathbf{r}') \delta(t - t') \hat{\mathbf{e}}_j$ in the direction of $\hat{\mathbf{e}}_j$. G_{ij}^E can then be directly computed from the Fourier transform of the resulting \mathbf{E} field. However, obtaining a smooth and decaying force integrand requires expressing the mapping $\omega \rightarrow \omega(\xi)$ in the time-domain equations of motion. A simple way to see the effect of this mapping is to notice that Eq. (9) can be viewed as the Green's function at real "frequency" ξ and complex dielectric [50],

$$\varepsilon_c(\mathbf{r}, \xi) = \frac{\omega^2(\xi)}{\xi^2} \varepsilon(\mathbf{r}), \quad (13)$$

where for simplicity we have taken μ and ε to be frequency independent. We assume this to be the case for the remainder of the paper. At this point, it is important to emphasize that the original physical system ε at a frequency ω is the one in which Casimir forces and fluctuations appear; the dissipative system ε_c at a frequency ξ is merely an artificial technique introduced to compute the Green's function.

Integrating along a frequency contour $\omega(\xi)$ is therefore equivalent to making the medium dispersive in the form of Eq. (13). Consequently, the time domain equations of motion

under this mapping correspond to evolution of the fields in an effective dispersive medium given by $\varepsilon_c(\mathbf{r}, \xi)$.

To be suitable for FDTD, this medium should have three properties: it must respect causality, it cannot support gain (which leads to exponential blowup in time-domain), and it should be easy to implement. A Wick rotation is very easy to implement in the time domain: it corresponds to setting $\varepsilon_c = -\varepsilon$. However, a negative epsilon represents gain (the refractive index is $\pm\sqrt{\varepsilon}$, where one of the signs corresponds to an exponentially growing solution). We are therefore forced to consider a more general, frequency-dependent ε_c .

Implementing arbitrary dispersion in FDTD generally requires the introduction of auxiliary fields or higher order time-derivative terms into Maxwell's equations, and can in general become computationally expensive [48]. The precise implementation will depend strongly on the choice of contour $\omega(\xi)$. However, almost any dispersion will suit our needs, as long as it is causal and dissipative (excluding gain). A simple choice is an $\varepsilon_c(\mathbf{r}, \xi)$ corresponding to a medium with frequency-independent conductivity σ ,

$$\varepsilon_c(\mathbf{r}, \xi) = \varepsilon(\mathbf{r}) \left(1 + \frac{i\sigma}{\xi} \right). \quad (14)$$

This has three main advantages: first, it is implemented in many FDTD solvers currently in use; second, it is numerically stable; and third, it can be efficiently implemented without an auxiliary differential equation [48]. In this case, the equations of motion in the time domain are given by

$$\frac{\partial \mu \mathbf{H}}{\partial t} = -\nabla \times \mathbf{E}, \quad (15)$$

$$\frac{\partial \varepsilon \mathbf{E}}{\partial t} = \nabla \times \mathbf{H} - \sigma \varepsilon \mathbf{E} - \mathbf{J}. \quad (16)$$

Writing the conductivity term as $\sigma \varepsilon$ is slightly nonstandard, but is convenient here for numerical reasons. In conjunction with Eqs. (3) and (4), and a Fourier transform in ξ , this yields a photon Green's function given by

$$\left[\nabla \times \frac{1}{\mu(\mathbf{r})} \nabla \times - \xi^2 \varepsilon(\mathbf{r}) \left(1 + \frac{i\sigma}{\xi} \right) \right] \mathbf{G}_j(\xi; \mathbf{r}, \mathbf{r}') = \delta(\mathbf{r} - \mathbf{r}') \hat{\mathbf{e}}_j, \quad (17)$$

This corresponds to picking a frequency contour of the form

$$\omega(\xi) \equiv \xi \sqrt{1 + \frac{i\sigma}{\xi}}, \quad (18)$$

Note that, in the time domain, the frequency of the fields is ξ , and not ω , i.e., their time dependence is $e^{-i\xi t}$. The only role of the conductivity σ here is to introduce an imaginary component to Eq. (17) in correspondence with a complex-frequency mapping. It also explicitly appears in the final expression for the force, Eq. (12), as a multiplicative (Jacobian) factor.

The standard FDTD method involves a discretized form of Eqs. (15) and (16), from which one obtains \mathbf{E} and \mathbf{B} , not G_{ij}^E . However, in the frequency domain, the photon Green's

function, being the solution to Eq. (6), solves exactly the same equations as those satisfied by the electric field \mathbf{E} , except for a simple multiplicative factor in Eq. (3). Specifically, G_{ij}^E is given in terms of \mathbf{E} by

$$G_{ij}^E(\xi; \mathbf{r}, \mathbf{r}') = -\frac{E_{i,j}(\mathbf{r}, \xi)}{i\xi\mathcal{J}(\xi)}, \quad (19)$$

where $E_{i,j}(\mathbf{r}, \xi)$ denotes the field in the i th direction due to a dipole current source $\mathbf{J}(\mathbf{r}, t) = \mathcal{J}(t)\delta(\mathbf{r}-\mathbf{r}')\hat{\mathbf{e}}_j$ placed at \mathbf{r}' with time-dependence $\mathcal{J}(t)$, e.g., $\mathcal{J}(t) = \delta(t)$.

In principle, we can now compute the electric- and magnetic-field correlation functions by using Eqs. (10) and (11), with $\omega(\xi)$ given by Eq. (18), and by setting $\mathbf{r}=\mathbf{r}'$ in Eq. (11). Since we assume a discrete spatial grid, no singularities arise for $\mathbf{r}=\mathbf{r}'$, and in fact any \mathbf{r} -independent contribution is canceled upon integration over S . This is straightforward for Eq. (7) since the \mathbf{E} -field correlation function only involves a simple multiplication by $\omega^2(\xi)$. However, the \mathbf{H} -field correlation function, Eq. (8), involves derivatives in space. Although it is possible to compute these derivatives numerically as finite differences, it is conceptually much simpler to pick a different vector potential, analogous to Eqs. (3) and (4), in which \mathbf{H} is the time-derivative of a vector potential \mathbf{A}^H . As discussed in the Appendix, this choice of vector potential implies a frequency-independent magnetic conductivity, and a magnetic, instead of electric, current. The resulting time-domain equations of motion are

$$\frac{\partial \mu \mathbf{H}}{\partial t} = -\nabla \times \mathbf{E} + \sigma \mu \mathbf{H} - \mathbf{J}, \quad (20)$$

$$\frac{\partial \varepsilon \mathbf{E}}{\partial t} = \nabla \times \mathbf{H}. \quad (21)$$

In this gauge, the new photon Green's function $G_{ij}^H = \langle A_i^H(\mathbf{r}, \xi) A_j^H(\mathbf{r}', \xi) \rangle$ and the field \mathbf{H} in response to the current source \mathbf{J} are related by

$$G_{ij}^H(\xi; \mathbf{r}, \mathbf{r}') = -\frac{H_{i,j}(\mathbf{r}, \xi)}{i\xi\mathcal{J}(\xi)}, \quad (22)$$

where the magnetic-field correlation function,

$$\langle H_i(\mathbf{r}, \xi) H_j(\mathbf{r}', \xi) \rangle = \frac{\hbar}{\pi} \omega^2(\xi) G_{ij}^H(\xi; \mathbf{r}, \mathbf{r}'), \quad (23)$$

is now defined as a frequency multiple of G_{ij}^H rather than by a spatial derivative of G_{ij}^E .

This approach to computing the magnetic correlation function has the advantage of treating the electric and magnetic fields on the same footing, and also allows us to examine only the field response at the location of the current source. The removal of spatial derivatives also greatly simplifies the incorporation of discretization into our equations (see Appendix for further discussion). The use of magnetic currents and conductivities, while unphysical, are easily implemented numerically. Alternatively, one could simply interchange ε and μ , \mathbf{E} and \mathbf{H} , and run the simulation entirely as in Eqs. (15) and (16).

The full force integral is then expressed in the symmetric form

$$F_i = \text{Im} \frac{\hbar}{\pi} \int_{-\infty}^{\infty} d\xi g(\xi) [\Gamma_i^E(\xi) + \Gamma_i^H(\xi)], \quad (24)$$

where

$$\Gamma_i^E(\xi) \equiv \iint_S \sum_j \varepsilon(\mathbf{r}) \left(E_{i,j}(\mathbf{r}) - \frac{1}{2} \delta_{ij} \sum_k E_{k,k}(\mathbf{r}) \right) dS_j, \quad (25)$$

$$\Gamma_i^H(\xi) \equiv \iint_S \sum_j \frac{1}{\mu(\mathbf{r})} \left(H_{i,j}(\mathbf{r}) - \frac{1}{2} \delta_{ij} \sum_k H_{k,k}(\mathbf{r}) \right) dS_j \quad (26)$$

represent the surface-integrated field responses in the frequency domain, with $E_{i,j}(\mathbf{r}) \equiv E_{i,j}(\mathbf{r}; \xi)$. For notational simplicity, we have also defined

$$g(\xi) \equiv \frac{\omega^2}{i\xi\mathcal{J}(\xi)} \frac{d\omega}{d\xi} \Theta(\xi). \quad (27)$$

Here, the path of integration has been extended to the entire real ξ axis with the use of the unit-step function $\Theta(\xi)$ for later convenience.

The product of the fields with $g(\xi)$ naturally decomposes the problem into two parts: computation of the surface integral of the field correlations Γ , and of the function $g(\xi)$. The Γ_i 's contain all the structural information, and are straightforward to compute as the output of any available FDTD solver with no modification to the code. This output is then combined with $g(\xi)$, which is easily computed analytically, and integrated in Eq. (24) to obtain the Casimir force. As discussed in Sec. IVA, the effect of spatial and temporal discretization enters explicitly only as a slight modification to $g(\xi)$ in Eq. (24), leaving the basic conclusions unchanged.

D. Evaluation in the time domain

It is straightforward to evaluate Eq. (24) in the frequency domain via a dipole current $\mathcal{J}(t) = \delta(t)$, which yields a constant-amplitude current $\mathcal{J}(\xi) = 1$. Using the frequency-independent conductivity contour Eq. (18), corresponding to Eqs. (15) and (16), we find the following explicit form for $g(\xi)$:

$$g(\xi) = -i\xi \left(1 + \frac{i\sigma}{\xi} \right) \frac{1 + i\sigma/2\xi}{\sqrt{1 + i\sigma/\xi}} \Theta(\xi). \quad (28)$$

One important feature of Eq. (28) is that $g(\xi) \rightarrow \sqrt{i\sigma^3/\xi}$ becomes singular in the limit as $\xi \rightarrow 0$. Assuming that $\Gamma^E(\xi)$ and $\Gamma^H(\xi)$ are continuous at $\xi=0$ (in general they will not be zero), this singularity is integrable. However, it is cumbersome to integrate in the frequency domain, as it requires careful consideration of the time window for calculation of the field Fourier transforms to ensure accurate integration over the singularity.

As a simple alternative, we use the convolution theorem to re-express the frequency (ξ) integral of the product of $g(\xi)$

and $\Gamma^E(\xi)$ arising in Eq. (24) as an integral over time t of their Fourier transforms $g(-t)$ and $\Gamma^E(t)$. Technically, the Fourier transform of $g(\xi)$ does not exist because $g(\xi) \sim \xi$ for large ξ . However, the integral is regularized below using the time discretization, just as the Green's function above was regularized by the spatial discretization. (As a convenient abuse of notation, ξ arguments will always denote functions in the frequency domain, and t arguments their Fourier transforms in the time domain.)

Taking advantage of the causality conditions [$\Gamma^E(t)$, $\Gamma^H(t)=0$ for $t<0$] yields the following expression for the force expressed purely in the time domain:

$$F_i = \text{Im} \frac{\hbar}{\pi} \int_0^\infty dt g(-t) [\Gamma_i^E(t) + \Gamma_i^H(t)]. \quad (29)$$

The advantage of evaluating the force integral in the time domain is that, due to the finite conductivity and lack of sources for $t>0$, $\Gamma(t)$ will rapidly decay in time. As will be shown in the next section, $g(-t)$ also decays with time. Hence, although dissipation was originally introduced to permit a natural high-frequency cutoff to our computations, it also allows for a natural time cutoff T . We pick T such that, for times $t>T$, knowledge of the fields will not change the force result in Eq. (29) beyond a predetermined error threshold. This approach is very general as it requires no precise knowledge of how the fields decay with time.

E. Properties of $g(-t)$

Given $g(\xi)$, the desired function $g(-t)$ is a Fourier transform. However, the discretization of time in FDTD implies that the frequency domain becomes periodic and that $g(t) = g(n\Delta t)$ are actually Fourier series coefficients, given by

$$g(n\Delta t) = \int_0^{2\pi/\Delta t} d\xi g_d(\xi) e^{-i\xi n\Delta t}, \quad (30)$$

where $g_d(\xi)$ is the discretized form of Eq. (27) and is given in the Appendix by Eq. (38). These Fourier series coefficients are computed by a sequence of numeric integrals that can be evaluated in a variety of ways. It is important to evaluate them accurately in order to resolve the effect of the $\xi=0$ singularity. For example, one could use a Clenshaw-Curtis scheme developed specifically for Fourier integrals [55], or simply a trapezoidal rule with a large number of points that can be evaluated relatively quickly by a fast Fourier transform [e.g., for this particular $g(\xi)$, 10^7 points is sufficient].

Since it is possible to employ strictly real current sources in FDTD, giving rise to real Γ , and since we are only interested in analyzing the influence of $g(t)$ on Eq. (29), it suffices to look at $\text{Im} g(-t)$. Furthermore, $g(t)$ will exhibit rapid oscillations at the Nyquist frequency due to the delta-function current, and therefore it is more convenient to look at its absolute value. Figure 1, below, plots the envelope of $|\text{Im} g(-t)|$ as a function of t , where again, $g(t)$ is the Fourier transform of Eq. (27).

As anticipated in the previous section, $g(t)$ decays in time. Interestingly, it exhibits a transition from $\sim t^{-1}$ decay at σ

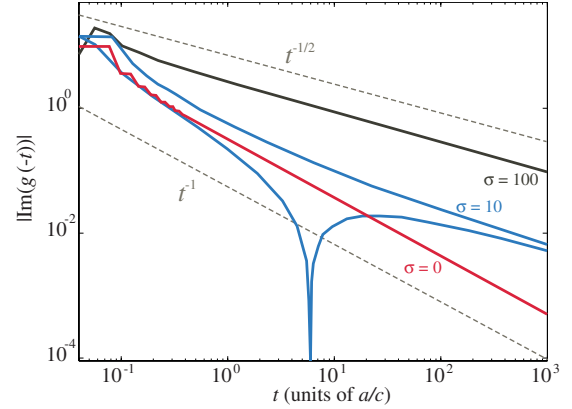


FIG. 1. (Color online) $|\text{Im} g(t)|$ for various values of σ , illustrating the transition from t^{-1} to $t^{-1/2}$ power-law decay as σ increases. Because there are strong oscillations in $g(t)$ at the Nyquist frequency for intermediate σ , for clarity we plot the positive and negative terms in $g(t)$ as separate components.

$=0$ to $\sim t^{-1/2}$ decay for large σ . The slower decay at long times for larger σ arises from a transition in the behavior of Eq. (28) from the singularity at $\xi=0$.

III. PROPERTIES OF THE METHOD

In this section we discuss the practical implementation of the time-domain algorithm (using a freely available time-domain solver [51] that required no modification). We analyze its properties applied to the simplest parallel-plate geometry [Fig. 2], which illustrate the essential features in the simplest possible context. In particular, we analyze important computational properties such as the convergence rate and the impact of different conductivity choices. A forthcoming of this paper, in preparation, demonstrates the method for more complicated two- and three-dimensional geometries [52].

A. Fields in real time

The dissipation due to positive σ implies that the fields, and hence $\Gamma^E(t)$, will decay exponentially with time. Below,

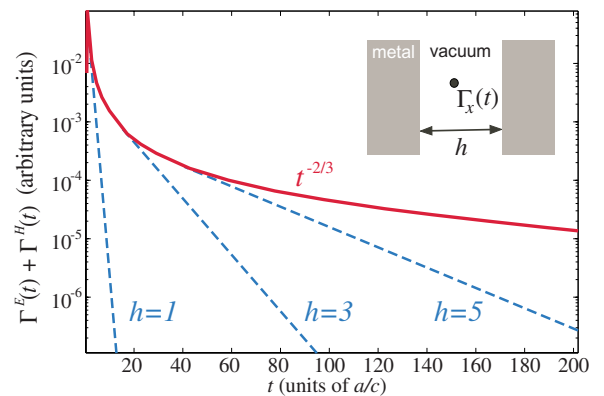


FIG. 2. (Color online) $\Gamma_x^E(t) + \Gamma_x^H(t)$ for a set of one-dimensional parallel plates as the separation h is varied. The inset shows the physical setup.

we use a simple one-dimensional example to understand the consequences of this dissipation for both the one-dimensional parallel plates and the two-dimensional piston configuration. The simplicity of the parallel-plate configuration allows us to examine much of the behavior of the time-domain response analytically. (The understanding gained from the one-dimensional geometry can be applied to higher dimensions.) Furthermore, we confirm that the error in the Casimir force due to truncating the simulation at finite time decreases exponentially (rather than as t^{-1} , as it would for no dissipation).

1. One-dimensional parallel plates

To gain a general understanding of the behavior of the system in the time domain, we first examine a simple configuration of perfectly metallic parallel plates in one dimension. The plates are separated by a distance h (in units of an arbitrary distance a) in the x dimension, as shown by the inset of Fig. 2. The figure plots the field response $\Gamma_x^E(t) + \Gamma_x^H(t)$, in arbitrary units, to a current source $\mathcal{J}(t) = \delta(t)$ for increasing values of h , with the conductivity set at $\sigma = 10(2\pi c/a)$.

Figure 2 shows the general trend of the field response as a function of separation. For short times, all fields follow the same power-law envelope, and later rapidly transition to exponential decay. Also plotted for reference is a $t^{-3/2}$ curve, demonstrating that the envelope is in fact a power law.

We can understand the power-law envelope by considering the vacuum Green’s function G^E in the case $h \rightarrow \infty$ (analogous conclusions hold for G^H). In the case $h \rightarrow \infty$, one can easily solve for the vacuum Green’s function $G^E(\xi, \mathbf{r} - \mathbf{r}')$ in one dimension for real frequency ξ ,

$$G^E(\xi, \mathbf{r} - \mathbf{r}') = \frac{e^{i\xi|\mathbf{r}-\mathbf{r}'|}}{i\xi}. \tag{31}$$

We then analytically continue this expression to the complex-frequency domain via Eq. (18) and compute the Fourier transform $\int d\xi e^{i\xi t} G^E(\omega(\xi))$. Setting $\mathbf{r} = \mathbf{r}'$ in the final expression, one finds that, to leading order, $G^E(t) \sim t^{-3/2}$. This explains the behavior of the envelope in Fig. 2 and the short-time behavior of the Green’s functions: it is the field response of vacuum.

Intuitively, the envelope decays only as a power in t because it receives contributions from a continuum of modes, all of which are individually decaying exponentially (this is similar to the case of the decay of correlations in a thermodynamic system near a critical point [56]). For a finite cavity, the mode spectrum is discrete—the poles in the Green’s function of the nondissipative physical system are pushed below the real-frequency axis in this dissipative, unphysical system, but they remain discretely spaced.

At short times, the field response of a finite cavity will mirror that of an infinite cavity because the fields have not yet propagated to the cavity walls and back. As t increases, the cavity response will transition to a discrete sum of exponentially decaying modes. From Eq. (18), higher-frequency modes have a greater imaginary-frequency component, so at sufficiently long times the response will decay exponentially,

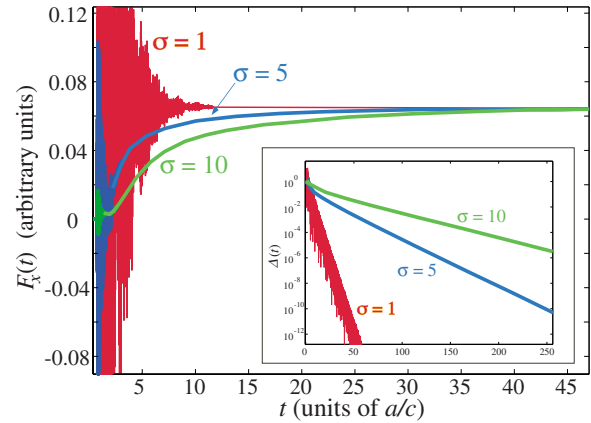


FIG. 3. (Color online) Partial force as defined in Eq. (32) for one-dimensional parallel plates as a function of time t . (Inset): Relative error $\Delta(t)$ as a function of t on a semilogarithmic scale.

the decay being determined by the lowest-frequency cavity mode. The higher the frequency of that mode, the faster the dissipation.

This prediction is confirmed in Fig. 2: as h decreases, the source “sees” the walls sooner. From the standpoint of computational efficiency, this method then works best when objects are in close proximity to one another (although not so close that spatial resolution becomes an issue), a situation of experimental interest.

2. Convergence of the force

We now examine the force on the parallel plates. From the above discussions of the field decay and the decay of $g(t)$, we expect the time integral in Eq. (29) to eventually converge exponentially as a function of time. In the interest of quantifying this convergence, we define the time dependent “partial force” $F_i(t)$ as

$$F_i(t) \equiv \text{Im} \frac{\hbar}{\pi} \int_0^t dt' g(-t') [\Gamma_i^E(t') + \Gamma_i^H(t')]. \tag{32}$$

Letting $F_i(\infty)$ denote the $t \rightarrow \infty$ limit of $F_i(t)$, which is the actual Casimir force, we define the relative error $\Delta_i(t)$ in the i th component of the force as

$$\Delta_i(t) \equiv \left| \frac{F_i(t) - F_i(\infty)}{F_i(\infty)} \right|. \tag{33}$$

We plot $F_x(t)$ in Fig. 3 for the one-dimensional parallel-plate structure with different values of σ . The inset plots $\Delta(t)$ for the same configuration. As expected, the asymptotic value of $F_x(t)$ is independent of σ , and $\Delta(t)$ converges exponentially to zero.

For σ near zero, the force is highly oscillatory. In one dimension this gives the most rapid convergence with time, but it is problematic in higher dimensions. This is because, in higher-dimensional systems, S consists of many points, each contributing a response term as in Fig. 3. If σ is small, every one of these terms will be highly oscillatory, and the correct

force Eq. (32) will only be obtained through delicate cancellations at all points on S . Small σ is thus very sensitive to numerical error.

Increasing σ smoothes out the response functions, as higher-frequency modes are damped out. However, somewhat counterintuitively, it also has the effect of slowing down the exponential convergence. One can understand the asymptotic behavior of the force by considering the equations of motion Eq. (17) as a function of σ and ξ . When the response function exhibits few if any oscillations we are in the regime where $\sigma \gg \xi$. In this limit, the approximate equations of motion are

$$\left[\nabla \times \frac{1}{\mu(\mathbf{r})} \nabla \times - i\sigma \xi \varepsilon(\mathbf{r}) \right] \mathbf{G}_j(\xi; \mathbf{r}, \mathbf{r}') = \delta(\mathbf{r} - \mathbf{r}') \hat{\mathbf{e}}_j. \quad (34)$$

In the limit of Eq. (34), the eigenfrequency ξ of a given spatial mode scales proportional to $-i/\sigma$. The lowest-frequency mode therefore has a time-dependence $\sim e^{-Ct/\sigma}$, for some constant $C > 0$. Since the decay of the force at long times is determined by this mode, we expect the decay time to scale inversely with σ in the limit of very high σ . This is suggested in Fig. 3 and confirmed by further numerical experiments.

Additionally, from Eq. (34) we see that in the case of a homogeneous one-dimensional cavity, the solutions have a quadratic dispersion $\xi \sim ik^2$, for spatial dependence e^{ikx} , and so the lowest cavity frequency scales as the inverse square of the cavity size. This means that the rate of exponential convergence of Fig. 2 should vary as $\sim h^{-2}$ in the limit of very large σ . This scaling is approximately apparent from Fig. 2, and further experiments for much larger σ confirm the scaling. We thus see that in this limit, the effect of increasing σ by some factor is analogous to increasing the wall spacing of the cavity by the square root of that factor.

The present analysis shows that there are two undesirable extremes. When σ is small, rapid oscillations in $F_i(t)$ will lead to large numerical errors in more than one dimension. When σ is large, the resulting frequency shift will cause the cavity mode to decay more slowly, resulting in a longer run time. The optimal σ lies somewhere in between these two extremes and will generally depend on the system being studied. For the systems considered in this paper, with a typical scale $\approx a$, $\sigma \sim 1$ ($2\pi c/a$) appears to be a good value for efficient and stable time-domain computation.

IV. CONCLUDING REMARKS

An algorithm to compute Casimir forces in FDTD has several practical advantages. FDTD algorithms that solve Maxwell's equations with frequency-independent conductivity, and even more complicated dispersions, are plentiful and well-studied. They are stable, convergent, and easily parallelized. Although the current formulation of our method requires the evaluation of $G_{ij}(\mathbf{r})$ along a surface S , requiring a separate calculation of the fields for each dipole source in S , all of these sources can be simulated in parallel, with no communication between different simulations until the very

end of the computation. In addition, many FDTD solvers will allow the computational cell for each source to be parallelized, providing a powerful method capable of performing large computations.

The calculations of this paper employed nondispersive materials in the original (ω) system. However, the theoretical analysis applies equally well to materials of arbitrary dispersion. Any materials that can be implemented in an FDTD solver (e.g., a sum of Lorentzian dielectric resonances [48]) can also be included, and existing algorithms have demonstrated the ability to model real materials [48,57]. Existing FDTD implementations also handle anisotropy in ε and μ , multiple types of boundary conditions, and other complications [48].

In principle, the computational scaling of this FDTD method is comparable to finite-difference frequency-domain (FDFD) methods [30]. In both cases, each solver step (either a time step for FDTD or an iterative-solver step for FDFD) requires $O(N)$ work for N grid points. The number of time steps required by an FDTD method is proportional to the diameter of the computational cell, or $N^{1/d}$ in d dimensions. With an ideal multigrid solver, FDFD can in principle be solved by $O(1)$ solver steps, but a simpler solver like conjugate gradient requires a number of steps proportional to the diameter as well [30]. In both cases, the number of points to be solved on the surface S is $O(N^{1-1/d})$. Hence, the overall complexity of the simplest implementations (not multigrid) is $O(N^2)$. We believe that future boundary-element methods [30,37] will achieve better efficiency, but such methods require considerable effort to implement and their implementation is specific to the homogeneous-medium Green's function, which depends on the boundary conditions, dimensionality, and types of materials considered [58].

A planned subsequent article [52], will illustrate the method in various nontrivial two- and three-dimensional geometries, including dispersive dielectrics. In addition, we present an optimization of our method (based on a rapidly converging series expansion of the fields) that greatly speeds up the spatial integral of the stress tensor. We also compute forces in three-dimensional geometries with cylindrical symmetry, which allows us to take advantage of the cylindrical coordinates support in existing FDTD software [51] and employ a two-dimensional computational cell.

ACKNOWLEDGMENTS

We would like to thank Peter Bermel and Ardavan Farjadpour for useful discussions. This work was supported by the Army Research Office through the ISN under Contract No. W911NF-07-D-0004, the MIT Ferry Fund, and by U.S. DOE Grant No. DE-FG02-97ER25308 (A.W.R.).

APPENDIX

1. Temporal discretization

FDTD algorithms approximate both time and space by a discrete uniform mesh. Bearing aside the standard analysis of stability and convergence [48], this discretization will slightly modify the analysis in the preceding sections. In par-

ticular, the use of a finite temporal grid (resolution Δt) implies that all continuous time derivatives are now replaced by a finite-difference relation, which in the case of Maxwell's equations is commonly taken to be a forward difference

$$\frac{\partial f}{\partial t} \approx \frac{f_i(\mathbf{r}, t + \Delta t) - f_i(\mathbf{r}, t)}{\Delta t} \equiv \partial_t^{(d)} f, \quad (\text{A1})$$

where $f(t)$ is an arbitrary function of time. The effect of temporal discretization is therefore to replace the linear operator $\partial/\partial t$ with $\partial_t^{(d)}$. The representation of this operator is simple to compute in the frequency domain. Letting $\partial_t^{(d)}$ act on a Fourier component of $f(t)$ yields

$$\partial_t^{(d)} e^{-i\xi t} = -i\xi_d e^{-i\xi t}, \quad (\text{A2})$$

where

$$\xi_d(\xi) \equiv \frac{2}{\Delta t} \sin\left(\frac{\xi \Delta t}{2}\right) e^{-i\frac{\xi \Delta t}{2}} \quad (\text{A3})$$

The effect of discretization on the system is thus to replace $i\xi$ by $i\xi_d$ in the derivatives, which corresponds to numerical dispersion arising from the ultraviolet (Nyquist) frequency cutoff $\pi/\Delta t$. This not only affects the solutions to Eqs. (15) and (16), but also the complex-frequency mapping of Eq. (18): the mapping $\xi \rightarrow \omega(\xi) = \xi\sqrt{1+i\sigma/\xi}$ becomes $\xi \rightarrow \omega_d(\xi) = \xi_d\sqrt{1+i\sigma/\xi_d}$. Note that ξ is still the frequency parameter governing the time dependence of the Fourier components of $f(t)$ and $\xi_d \rightarrow \xi$ in the limit of infinite resolution ($\Delta t \rightarrow 0$). In this limit, our original mapping is restored and FDTD yields the correct temporal evolution of the fields. In practice, accurate convergence is achieved for reasonable resolutions, because Casimir forces are dominated by frequency contributions much smaller than the Nyquist frequency. The dominant frequency contributions to the Casimir force are bounded from above by a frequency $\sim 1/\ell$, where ℓ is determined by a typical lengthscale, e.g., body sizes and separations.

Because FDTD is convergent [$\xi_d = \xi + O(\Delta t^2)$], most of the analysis can be performed (as in this paper) in the $\Delta t \rightarrow 0$ limit. However, care must be taken in computing $g(t)$ because the Fourier transform of $g(\xi)$, Eq. (27), does not exist as $\Delta t \rightarrow 0$. We must compute it in the finite Δt regime. In particular, the finite resolution requires, via Eq. (37), that we replace $g(\omega)$ in Eq. (27) by

$$g_d(\xi) \equiv \frac{\omega_d^2}{i\xi_d \mathcal{J}(\xi)} \frac{d\omega}{d\xi}. \quad (\text{A4})$$

Note that the Jacobian factor $d\omega/d\xi$ involves ω and ξ , not $\omega_d(\xi) = \xi_d\sqrt{1+i\sigma/\xi_d}$ and ξ_d , although of course the latter converge to the former as $\Delta t \rightarrow 0$. The basic principle is that one must be careful to use the discrete analogs to continuous solutions in cases where there is a divergence or regularization needed. This is the case for $g(\xi)$, but not for the Jacobian.

Similarly, if one wished to subtract the vacuum Green's function from the Green's function, one needs to subtract the vacuum Green's function as computed in the discretized vacuum. Such a subtraction is unnecessary if the stress tensor is integrated over a closed surface (vacuum contributions are

constants that integrate to zero), but is useful in cases such as the parallel plates considered here. By subtracting the (discretized) vacuum Green's function, one can evaluate the stress tensor only for a single point between the plates, rather than for a "closed surface" with another point on the other side of the plates [2].

As was noted before Eq. (30), the Nyquist frequency $\pi/\Delta t$ regularizes the frequency integrations, similar to other ultraviolet regularization schemes employed in Casimir-force calculations [59,60]. Because the total frequency integrand in Eq. (1) goes to zero for large ξ (due to cancellations occurring in the spatial integration and also due to the dissipation introduced in our approach), the precise nature of this regularization is irrelevant as long as Δt is sufficiently small (i.e., at high enough resolution).

2. Magnetic correlation function

One way to compute the magnetic correlation function is by taking spatial derivatives of the electric Green's function by Eq. (8), but this is inefficient because a numerical derivative involves evaluating the electric Green's function at multiple points. Instead, we compute the magnetic Green's function directly, finding the magnetic field in response to a magnetic current. This formulation, however, necessitates a change in the choice of vector potentials [Eqs. (3) and (4)] as well as a switch from electric to magnetic conductivity, for reasons explained in this section.

Equations (3) and (4) express the magnetic field \mathbf{B} as the curl of the vector potential \mathbf{A}^E , enforcing the constraint that \mathbf{B} is divergence free (no magnetic charge). However, this is no longer true when there is a magnetic current, as can be seen by taking the divergence of both sides of Faraday's law with a magnetic current \mathbf{J} , $\partial\mathbf{B}/\partial t = -\nabla \times \mathbf{E} - \mathbf{J}$, since $\nabla \cdot \mathbf{J} \neq 0$ for a point-dipole current \mathbf{J} . Instead, because there need not be any free electric charge in the absence of an electric current source, one can switch to a new vector potential \mathbf{A}^H such that

$$\varepsilon E_i(\mathbf{r}, \omega) = (\nabla \times)_{ij} A_j^H(\mathbf{r}, \omega), \quad (\text{A5})$$

$$H_i(\mathbf{r}, \omega) = -i\omega A_i^H(\mathbf{r}, \omega). \quad (\text{A6})$$

The desired correlation function is then given, analogous to Eq. (7), by

$$\langle H_i(\mathbf{r}, \omega) H_j(\mathbf{r}', \omega) \rangle = \frac{\hbar}{\pi} \omega^2 \text{Im} G_{ij}^H(\omega; \mathbf{r}, \mathbf{r}'), \quad (\text{A7})$$

where the photon magnetic Green's function G^H solves [similar to Eq. (6)]

$$\left[\nabla \times \frac{1}{\varepsilon(\mathbf{r}, \omega)} \nabla \times - \omega^2 \mu(\mathbf{r}, \omega) \right] \mathbf{G}_j^H(\omega; \mathbf{r}, \mathbf{r}') = \delta(\mathbf{r} - \mathbf{r}') \hat{\mathbf{e}}_j. \quad (\text{A8})$$

Now, all that remains is to map Eq. (A8) onto an equivalent real-frequency (ξ) system that can be evaluated in the time domain, similar to Sec. II C, for $\omega(\xi)$ given by Eq. (18). There are at least two ways to accomplish this. One possibility, which we have adopted in this paper, is to define an

effective magnetic permeability $\mu_c = \mu \omega^2(\xi) / \xi^2$, corresponding to a *magnetic* conductivity, similar to Eq. (13). Combined with Eq. (18), this directly yields a magnetic conductivity as in Eq. (20).

A second possibility is to divide both sides of Eq. (A8) by $\omega^2 / \xi^2 = 1 + i\sigma / \xi$, and absorb the $1 + i\sigma / \xi$ factor into ε via Eq. (13). That is, one can compute the magnetic correlation function via the magnetic field in response to a magnetic current with an *electric* conductivity. However, the magnetic current in this case has a frequency response that is divided by $1 + i\sigma / \xi$, which is simply a rescaling of $\mathcal{J}(\xi)$ in Eq. (22). There is no particular computational advantage to this alternative, but for an experimental realization [50], an electric conductivity is considerably more attractive. [Note that rescaling $\mathcal{J}(\xi)$ by $1 + i\sigma / \omega$ will yield a new $g(\xi)$ in Eq. (27), corresponding to a new $g(t)$ that exhibits slower decay.]

3. Material dispersion

In this section, we extend the time-domain formalism presented above to cases where the dielectric permittivity of the medium of interest is dispersive. To begin with, note that in this case the dissipative, complex dielectric ε_c of Eq. (43) is given by

$$\varepsilon_c(\mathbf{r}, \xi) = \frac{\omega^2(\xi)}{\xi^2} \varepsilon(\mathbf{r}, \omega(\xi)), \quad (\text{A9})$$

where $\varepsilon(\mathbf{r}, \omega(\xi))$ denotes the permittivity of the geometry of interest evaluated over the complex contour $\omega(\xi)$.

This complex dielectric manifests itself as a convolution in the time-domain equations of motion, i.e., in general, $\mathbf{D}(t) = \int dt' \varepsilon_c(t-t') \mathbf{E}(t')$. The standard way to implement this in FDTD is to employ an auxiliary equation of motion for the polarization [57]. For the particular contour chosen in this paper [Eq. (18)], the conductivity term already includes the prefactor ω^2 / ξ^2 and therefore one need only add the dispersion due to $\varepsilon(\mathbf{r}, \omega(\xi))$.

The only other modification to the method comes from the dependence of $\Gamma^E(\xi)$ in Eq. (25) on ε . We remind the reader that our definition of Γ was motivated by our desire to interpret Eq. (24) as the Fourier transform of the convolution of two quantities, and thus to express the Casimir force directly in terms of the electric and magnetic fields $\mathbf{E}(t)$ and $\mathbf{H}(t)$, respectively. A straightforward generalization of Eq. (25) to dispersive media entails setting $\varepsilon(\mathbf{r}) \rightarrow \varepsilon(\mathbf{r}, \omega)$. However, in this case, the Fourier transform of Eq. (25) would be given by a convolution of $\mathbf{E}(\xi)$ and $\varepsilon(\mathbf{r} \in S, \omega(\xi))$ in the time domain, making it impossible to obtain $\Gamma^E(t)$ *directly* in terms of $\mathbf{E}(t)$. This is not a problem however, because the stress tensor *must* be evaluated over a surface S that lies entirely within a uniform medium (otherwise, S would cross a boundary and interpreting the result as a force on particular objects inside S would be problematic). The dielectric appearing in Eq. (25) is then at most a function of $\omega(\xi)$, i.e., $\varepsilon(\mathbf{r} \in S, \omega) = \varepsilon(\omega)$, which implies that we can simply absorb this factor into $g(\xi)$, modifying the numerical integral of Eq. (30). Furthermore, the most common case considered in Casimir-force calculations is one in which the stress tensor is evaluated in vacuum, i.e., $\varepsilon(\mathbf{r} \in S, \omega) = 1$, and thus dispersion does not modify $g(\xi)$ at all.

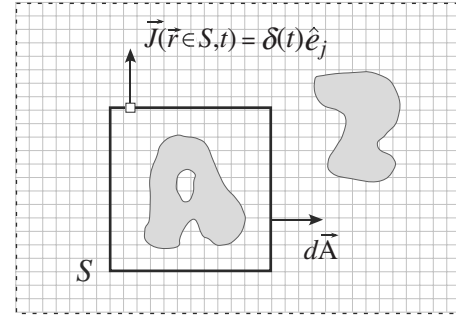


FIG. 4. Schematic of a possible contour around a body; the force on the body as computed by Eq. (44) involves an integral of the fields over the contour S .

4. Overview of the algorithm

In what follows, we summarize the time-domain Casimir method presented above, which leads to the following numerical algorithm to compute the Casimir force on an object:

(1) Pick a contour $\omega(\xi)$ over which to integrate the Casimir force. (For the class of contours considered here, Eq. (18), this corresponds to choosing a value for σ .)

(2) Pick a surface of integration S around the body of interest, depicted by the black contour in Fig. 4.

(3) Compute $g(n\Delta t)$, given by Eq. (30), by numerically integrating $g_d(\xi)$, given by Eq. (38). Note that the particular form of $g_d(\xi)$ will depend on $\omega(\xi)$, the temporal discretization Δt , the dielectric response at the surface of integration $\varepsilon(\mathbf{r} \in S, \omega) = \varepsilon(\omega)$, and the particular choice of current source—here, we only consider temporal delta-function current sources, i.e., $\mathcal{J}(\xi) = 1$. (Note that this step of the algorithm does not depend on geometry or the solution of the field equations. Thus, one can compute $g(n\Delta t)$ with very high accuracy and also store it for future use.)

(4) For every grid point $\mathbf{r} \in S$ on the discretized surface S , and for each polarization \hat{e}_j :

(a) Time-evolve Eqs. (15) and (16) and Eqs. (20) and (21) in response to a dipole current source $\mathbf{J}(\mathbf{r}, n\Delta t) = \mathcal{J}(n\Delta t) \hat{e}_j$, where $\mathcal{J}(n\Delta t) = \delta_{n,0} / \Delta t$ is the discretized version of a delta function.

(b) Obtain the electric $E_{i,j} = E_i(\mathbf{r}, n\Delta t)$ and magnetic $H_{i,j} = H_i(\mathbf{r}, n\Delta t)$ fields at position \mathbf{r} , and at each time step $n\Delta t$.

(c) Terminate the simulation once the fields have decayed beyond a desired error threshold (a time $T = N\Delta t$ determined by σ , as discussed in Sec. III A 2).

(5) Integrate $E_{i,j}$ and $H_{i,j}$ over the contour S to obtain $\Gamma_i^E(n\Delta t)$ and $\Gamma_i^H(n\Delta t)$, as in Eqs. (25) and (26). (Note that the spatial integral over the contour S is in fact a summation.)

(6) The force in the i th direction is given by a discretized form of Eq. (29),

$$F_i = \text{Im} \frac{\hbar}{\pi} \sum_{n=0}^N g(n\Delta t) [\Gamma_i^E(n\Delta t) + \Gamma_i^H(n\Delta t)]. \quad (\text{A10})$$

5. Spatial discretization

The FDTD algorithm involves a discretization of both space and time. The former leads to some subtleties in the

implementation of the above algorithm because the standard spatial discretization of FDTD is a *Yee lattice* in which different field components are discretized at different point in space [48]. For example, the grid for E_x is offset by half a pixel from the grids for E_y and H_z . This “staggered” grid is important to obtain second-order accuracy in discretizing the spatial derivatives, and also leads to other important properties of the algorithm [48]. However, it complicates the computation of the Casimir force because evaluating the stress tensor requires all components of the electric and magnetic fields to be evaluated at the same point.

The standard solution, which we use [51] and is also commonly implemented in FDTD software, is to simply linearly interpolate the different field components to the same point by averaging fields at adjacent grid points. As long as one interpolates to a point that is centered with respect to the different grids, such as the center of a pixel/voxel, this interpolation is second-order accurate. Accurate centered interpolation is especially important for Casimir forces because the net force involves delicate cancellations.

When a discontinuous boundary between two materials is discretized, the standard FDTD method becomes only first-order accurate, although there are schemes to restore second-order accuracy for both dielectric [51,61] and perfect-conductor [48,62] interfaces. There is an additional difficulty for Casimir calculations, however, because they involve a singular Green’s function. The Green’s function itself is always singular since we are evaluating the source and field at the same point, but ordinarily this singularity is subtracted out (for analytical regularizations) or in any case integrates to zero contribution to the net force [30]. Near an interface, however, there is an additional singularity due to reflection, which can be thought of as the singularity in the Green’s function of an image source on the other side of an interface [63]. Analytically, this additional term is not problematic since the stress-tensor integral must yield the same result

independent of the integration surface S , even if S is very close to a material interface. Numerically, on the other hand, we have observed that the additional singularity in the Green’s function exacerbates the spatial discretization error—the solution still converges at the same rate, $O(\Delta x)$ or $O(\Delta x^2)$ depending on which interface-discretization scheme is used, but the constant factor becomes larger as S approaches an interface. We dealt with this problem in two ways: first, we typically choose S to be midway between interfaces in order to maximize the distance from the interfaces. Second, we implemented the subtraction scheme described in Ref. [30], subtracting the stress integral for a second computation involving an isolated object for which the net force is theoretically zero, and we again observe that this greatly improves the constant coefficient in the convergence rate.

Finally, we should mention one pitfall to avoid in implementing the magnetic Green’s function. Two approaches to computing the magnetic Green’s function were described in Sec. IVB, but there is also a third approach. Since Maxwell’s equations are equivalent under interchange of \mathbf{E} and \mathbf{H} and ε and μ , one could compute the magnetic Green’s function by simply recomputing the electric Green’s function with ε and μ swapped (exchanging any perfect electric conductors for perfect magnetic conductors). However, because ε and μ are discretized slightly differently in a Yee-scheme FDTD implementation (due to the different grids of \mathbf{E} and \mathbf{H}), this approach can lead to subtle errors because it could change the volume of the objects being discretized. Even though the change in volume is of $O(\Delta x)$, the contribution from this change in volume need not converge to zero as $\Delta x \rightarrow 0$ because of the formally infinite energy density in the vacuum energy (due to the singularity of the Green’s function). Therefore, we recommend computing the magnetic Green’s function via the response to a magnetic current as described earlier.

-
- [1] H. B. G. Casimir, Proc. K. Ned. Akad. Wet. **51**, 793 (1948).
 [2] E. M. Lifshitz and L. P. Pitaevskii, *Statistical Physics: Part 2* (Pergamon, Oxford, 1980).
 [3] P. W. Milonni, *The Quantum Vacuum: An Introduction to Quantum Electrodynamics* (Academic Press, San Diego, 1993).
 [4] T. H. Boyer, Phys. Rev. A **9**, 2078 (1974).
 [5] S. K. Lamoreaux, Phys. Rev. Lett. **78**, 5 (1997).
 [6] U. Mohideen and A. Roy, Phys. Rev. Lett. **81**, 4549 (1998).
 [7] F. Chen, U. Mohideen, G. L. Klimchitskaya, and V. M. Mostepanenko, Phys. Rev. Lett. **88**, 101801 (2002).
 [8] H. B. Chan, V. A. Aksyuk, R. N. Kleinman, D. J. Bishop, and F. Capasso, Science **291**, 1941 (2001).
 [9] D. Iannuzzi, M. Lisanti, and F. Capasso, Proc. Natl. Acad. Sci. U.S.A. **101**, 4019 (2004).
 [10] D. Iannuzzi, M. Lisanti, J. Munday, and F. Capasso, Solid State Commun. **135**, 618 (2005).
 [11] P. A. Maia Neto, A. Lambrecht, and S. Reynaud, Europhys. Lett. **69**, 924 (2005).
 [12] M. Brown-Hayes, D. A. R. Dalvit, F. D. Mazzitelli, W. J. Kim, and R. Onofrio, Phys. Rev. A **72**, 052102 (2005).
 [13] M. Bordag, Phys. Rev. D **73**, 125018 (2006).
 [14] R. Onofrio, New J. Phys. **8**, 237 (2006).
 [15] T. Emig, Phys. Rev. Lett. **98**, 160801 (2007).
 [16] J. N. Munday and F. Capasso, Phys. Rev. A **75**, 060102(R) (2007).
 [17] M. Miri and R. Golestanian, Appl. Phys. Lett. **92**, 113103 (2008).
 [18] C. Genet, A. Lambrecht, and S. Reynaud, Eur. Phys. J. Spec. Top. **160**, 183 (2008).
 [19] J. Munday, F. Capasso, and V. A. Parsegia, Nature (London) **457**, 170 (2009).
 [20] G. L. Klimchitskaya, U. Mohideen, and V. M. Mostepanenko, e-print arXiv:0902.4022v1 Rev. Mod. Phys. (to be published).
 [21] B. Dobrich, M. DeKieviet, and H. Gies, Phys. Rev. D **78**, 125022 (2008).
 [22] M. Bordag, U. Mohideen, and V. M. Mostepanenko, Phys. Rep. **353**, 1 (2001).

- [23] K. A. Milton, *J. Phys. A* **37**, R209 (2004).
- [24] S. K. Lamoreaux, *Rep. Prog. Phys.* **68**, 201 (2005).
- [25] F. Capasso, J. N. Munday, D. Iannuzzi, and H. B. Chan, *IEEE J. Sel. Top. Quantum Electron.* **13**, 400 (2007).
- [26] H. B. Chan, Y. Bao, J. Zou, R. A. Cirelli, F. Klemens, W. M. Mansfield, and C. S. Pai, *Phys. Rev. Lett.* **101**, 030401 (2008).
- [27] T. Emig, A. Hanke, R. Golestanian, and M. Kardar, *Phys. Rev. Lett.* **87**, 260402 (2001).
- [28] H. Gies, K. Langfeld, and L. Moyaerts, *J. High Energy Phys.* **2003**, 018.
- [29] H. Gies and K. Klingmüller, *Phys. Rev. D* **74**, 045002 (2006).
- [30] A. Rodriguez, M. Ibanescu, D. Iannuzzi, J. D. Joannopoulos, and S. G. Johnson, *Phys. Rev. A* **76**, 032106 (2007).
- [31] S. J. Rahi, T. Emig, R. L. Jaffe, and M. Kardar, *Phys. Rev. A* **78**, 012104 (2008).
- [32] S. J. Rahi, A. W. Rodriguez, T. Emig, R. L. Jaffe, S. G. Johnson, and M. Kardar, *Phys. Rev. A* **77**, 030101(R) (2008).
- [33] T. Emig, N. Graham, R. L. Jaffe, and M. Kardar, *Phys. Rev. Lett.* **99**, 170403 (2007).
- [34] D. A. R. Dalvit, Paulo A. Maia Neto, A. Lambrecht, and S. Reynaud, *Phys. Rev. Lett.* **100**, 040405 (2008).
- [35] O. Kenneth and I. Klich, *Phys. Rev. B* **78**, 014103 (2008).
- [36] S. Reynaud, P. A. Maia Neto, and A. Lambrecht, *J. Phys. A: Math. Theor.* **41**, 164004 (2008).
- [37] H. T. M. Reid, A. W. Rodriguez, J. White, and S. G. Johnson, e-print arXiv:0904.0741v1, *Phys. Rev. Lett.* (unpublished).
- [38] S. Pasquali and A. C. Maggs, *Phys. Rev. A* **79**, 020102(R) (2009).
- [39] M. Antezza, L. P. Pitaevskiĭ, S. Stringari, and V. B. Svetovoy, *Phys. Rev. Lett.* **97**, 223203 (2006).
- [40] A. Rodriguez, M. Ibanescu, D. Iannuzzi, F. Capasso, J. D. Joannopoulos, and S. G. Johnson, *Phys. Rev. Lett.* **99**, 080401 (2007).
- [41] S. Zaheer, A. W. Rodriguez, S. G. Johnson, and R. L. Jaffe, *Phys. Rev. A* **76**, 063816 (2007).
- [42] A. W. Rodriguez, J. N. Munday, J. D. Joannopoulos, F. Capasso, D. A. R. Dalvit, and S. G. Johnson, *Phys. Rev. Lett.* **101**, 190404 (2008).
- [43] K. A. Milton, P. Parashar, and J. Wagner, *Phys. Rev. Lett.* **101**, 160402 (2008).
- [44] T. Emig, A. Hanke, R. Golestanian, and M. Kardar, *Phys. Rev. A* **67**, 022114 (2003).
- [45] M. P. Hertzberg, R. L. Jaffe, M. Kardar, and A. Scardicchio, *Phys. Rev. Lett.* **95**, 250402 (2005).
- [46] R. B. Rodrigues, Paulo A. Maia Neto, A. Lambrecht, and S. Reynaud, *Phys. Rev. Lett.* **96**, 100402 (2006).
- [47] D. A. R. Dalvit, F. C. Lombardo, F. D. Mazzitelli, and R. Onofrio, *Phys. Rev. A* **74**, 020101(R) (2006).
- [48] A. Taflove and S. C. Hagness, *Computational Electrodynamics: The Finite-Difference Time-Domain Method* (Artech, Norwood, MA, 2000).
- [49] F. S. S. Rosa, D. A. R. Dalvit, and P. W. Milonni, *Phys. Rev. A* **78**, 032117 (2008).
- [50] A. W. Rodriguez, A. P. McCauley, J. D. Joannopoulos, and S. G. Johnson, (unpublished).
- [51] A. Farjadpour, D. Roundy, A. Rodriguez, M. Ibanescu, P. Bermel, J. Burr, J. D. Joannopoulos, and S. G. Johnson, *Opt. Lett.* **31**, 2972 (2006).
- [52] A. P. McCauley, A. W. Rodriguez, J. D. Joannopoulos, and S. G. Johnson, e-print, arXiv:090.0267 (unpublished).
- [53] R. Barrett, M. Berry, T. F. Chan, J. Demmel, J. Donato, J. Dongarra, V. Eijkhout, R. Pozo, C. Romine, and H. Van der Vorst, *Templates for the Solution of Linear Systems: Building Blocks for Iterative Methods*, 2nd ed. (SIAM, Philadelphia, 1994).
- [54] L. N. Trefethen and D. Bau, *Numerical Linear Algebra*, 1st ed. (SIAM, Philadelphia, 1997).
- [55] R. Piessens, E. de Doncker-Kapenga, C. Uberhuber, and D. Hahaner, *QUADPACK: A Subroutine Package for Automatic Integration* (Springer-Verlag, Berlin, 1983).
- [56] N. Goldenfeld, *Lectures on Phase Transitions and the Renormalization Group* (Perseus Books, Reading, MA, 1992).
- [57] J. L. Young and R. O. Nelson, *IEEE Antennas Propag. Mag.* **43**, 61 (2001).
- [58] S. M. Rao and N. Balakrishnan, *Curr. Sci.* **77**, 1343 (1999).
- [59] E. M. Lifshitz, *Sov. Phys. JETP* **2**, 73 (1956).
- [60] F. D. Mazzitelli, D. A. Dalvit, and F. C. Lobardo, *New J. Phys.* **8**, 240 (2006).
- [61] A. Ditkowski, K. Dridi, and J. S. Hesthaven, *J. Comput. Phys.* **170**, 39 (2001).
- [62] I. A. Zagorodnov, R. Schuhmann, and T. Weiland, *Int. J. Numer. Model* **16**, 127 (2003).
- [63] J. D. Jackson, *Classical Electrodynamics*, 3rd ed. (Wiley, New York, 1998).